Adiabatic potential-energy surfaces of the H_2^+ ion in a strong magnetic field

U. Kappes
Theoretische Chemie, Physikalisch-Chemisches Institut, Im Neuenheimer Feld 253, 69120 Heidelberg, Federal Republic of Germany

P. Schmelcher
Physics Department, University of California, Santa Barbara, California 93106

(Received 30 June 1995)

We use a recently established and optimized atomic orbital basis set to perform extensive numerical calculations on the hydrogen molecular ion in a strong magnetic field. Many excited electronic states with gerade and ungerade parity as well as their potential-energy curves are investigated for the perpendicular configuration, i.e., for orthogonal internuclear and magnetic-field axes. The main issues of our investigation are the local as well as global topological properties of the potential-energy surfaces of the six energetically lowest electronic states of the H_2^+ ion in a strong magnetic field $B=1.0$ a.u. Our results show the existence of a variety of different possibilities for the topological behavior of the potential-energy surfaces: for the lowest electronic states the global equilibrium configuration is either the parallel or the perpendicular configuration, which are both distinguished by their higher symmetry. As a major result we observe, for the 3_u electronic state, the effect of a global symmetry lowering: the global equilibrium configuration of the 3_u potential-energy surface is at $\Theta=27°$, i.e., a configuration that strongly deviates from the distinct parallel or orthogonal configurations. Examinations of the electronic probability density distributions with varying angle Θ reveal the origin of the topological behavior of the different surfaces. [S1050-2947(96)07705-0]

PACS number(s): 32.10.−f

I. INTRODUCTION

Since the discovery of huge magnetic-field strengths on the surface of degenerate astrophysical objects [1], for example, white dwarfs (10^2–10^5 T) and neutron stars (10^7–10^9 T), the behavior and properties of matter exposed to such a strong magnetic field have been the subject of intensive theoretical studies. By means of theoretically calculated properties (spectra, oscillator strengths, etc.) of atoms and molecules in strong magnetic fields it is in principle possible to analyze the observational data from the above-mentioned cosmical objects. However, in the case of molecules our knowledge was, until the beginning of the 1990s, essentially restricted to the few lowest states of the H_2^+ ion [2–16]. For many electron molecules there exist only a few preliminary works [17–22] of qualitative character that deal mainly with the ground states of the corresponding molecules in particular in the very-high-field [23–26] regime.

The H_2^+ ion is of particular importance since it offers insight into the effects of an external magnetic field on the electronic structure and binding properties of diatomic molecules in general. Examples of such effects, which were already observed for the ground state of the H_2^+ ion, are the increase of the dissociation energy and the simultaneous decrease of the bond length with increasing magnetic-field strength. In particular the electronic energies are subject to principal modifications; the electronic potential energies of, for example, a diatomic molecule depend not only on the internuclear distance R but also on the angle Θ between the internuclear and magnetic-field axes. The properties of the H_2^+ ion in a strong magnetic field have so far been calculated predominantly for the case of the parallel configuration, i.e., $\Theta=0°$. By different numerical approaches it has been possible to investigate the lowest electronic states with orbital angular-momentum projections $|m|\leqslant 5$ for a wide range of magnetic-field strengths. With a recently established [27] and optimized [28] basis set of generalized atomic orbitals it has been possible to substantially improve and extend our knowledge on the properties of the excited states of the H_2^+ ion for the parallel configuration; the lowest electronic states with the magnetic quantum numbers $|m|\leqslant 10$ as well as many excited states within the subspaces for the magnetic quantum numbers $|m|=0,...,4$ were studied in detail [29,30]. As a particular result of these investigations the formation of a molecular bond by an external magnetic field has been observed; two classes of excited electronic states of the H_2^+ ion that are unbound in field-free space have been shown to bound above some critical field strength.

In contrast to the numerous studies on the H_2^+ ion for parallel internuclear and magnetic-field axes, there exists much less information about the behavior and properties of the H_2^+ ion for an arbitrary orientation of the molecule with respect to the magnetic field [13–16]. So far our knowledge on the *global* topological properties of the adiabatic electronic potential-energy surfaces is essentially restricted to the ground state of the H_2^+ ion, i.e., the 1_g state. The corresponding investigations have shown that the two-dimensional electronic potential-energy surface (PES) of the ground state of the H_2^+ ion leads to a much more interesting, but also more complicated, nuclear dynamics than in field-free space. The angle Θ, which is, in the absence of a magnetic field, a rotational degree of freedom, acquires increasing vibrational character with increasing magnetic-field strength, i.e., the H_2^+ ion is prevented from free rotation by a potential barrier and above some critical field strength rotation is possible only via a tunneling process. This effect is well known in the literature as the so-called hindered rotation [13,14,16].

Local properties of the PESs of excited states of the H_2^+ ion have been considered in the investigation by Wille [16]. Using a special basis-set method that is only applicable to one-electron molecular systems, it was possible to investigate the $1^+_{g/u}$, $2^+_{g/u}$, and $1^-_{g/u}$ states of the H_2^+ ion in a strong magnetic field $B=1.0$ a.u. for the orthogonal configuration, i.e., $\Theta=90°$. Some local properties of the topology of the lowest states of the H_2^+ ion were also investigated, i.e., the PESs considered were studied with respect to the dependence of the angle Θ for a fixed internuclear distance of 2.0 a.u. The disadvantage of the underlying basis-set method was the absence of gauge phases in the atomic orbital basis functions. These gauge phases have to be included in order to ensure the approximate gauge independence and in particular the correct gauge centering of the numerically calculated molecular wave functions and spectra. The phases are of particular importance for the dissociation limit of the molecule into atoms for which the gauge center of the orbitals has to be chosen on the individual nuclei [27]. For finite basis-set calculations the absence of a gauge-centering phase in the basis set leads to increasing inaccuracies with increasing internuclear distance R.

The aim of the present paper is to investigate the ground as well as many excited PESs of the H_2^+ ion in a strong homogeneous magnetic field $B=1.0$ a.u. With the aid of the above-mentioned optimized atomic orbital basis set, we investigate and discuss in detail the PESs of the six lowest electronic states of the H_2^+ ion. In addition, we also study a large number of electronic states for the orthogonal configuration ($\Theta=90°$), which is distinguished by its higher symmetry compared to the configurations with an arbitrary value of the angle Θ.

The paper is organized as follows. In Sec. II we briefly describe the symmetries of the well-known electronic Hamiltonian of the H_2^+ ion in the fixed-nuclei approach, followed by our method for the calculation of the molecular electronic wave functions and spectra. In Sec. III we present and discuss the results of our investigation for the orthogonal configuration. Finally, in Sec. IV we investigate and discuss in detail the PESs of the $1_{g/u}$, $2_{g/u}$, and $3_{g/u}$ states of the H_2^+ ion in a homogeneous magnetic field. Atomic units are used throughout ($B=1.0$ a.u. corresponds to 2.35×10^5 T).

II. PROPERTIES OF THE ELECTRONIC HAMILTONIAN AND NUMERICAL BASIS-SET METHOD

A full quantum-mechanical treatment of the motion of an electron and two protons under the influence of their mutual Coulomb interaction in the presence of a strong magnetic field is, at the moment, not feasible. Due to the nonzero net charge of the H_2^+ molecular system, the components of the conserved pseudomomentum do not commute, i.e., are not independent, and the center-of-mass coordinate cannot be completely eliminated from the total Hamiltonian [31–34] (a detailed discussion of the nonrelativistic Hamiltonian of the H_2^+ ion is given in Ref. [30]). Since we are primarily interested in the electronic structure of the H_2^+ ion, as a first step we have to separate the electronic and nuclear motion by the Born-Oppenheimer approximation in the presence of a magnetic field. This approximation, including all the mass corrections due to the finite nuclear masses, has been performed for neutral molecular systems in Ref. [35] and for molecular ions in Ref. [36].

In order to obtain the electronic Hamiltonian used in the present calculation, we introduce a further approximation: we choose as a zeroth-order approach infinitely heavy nuclei. Corrections going beyond the fixed-nuclei approach, i.e., the mass correction terms and the effects due to the center-of-mass motion, have been estimated for the ground, as well as for many excited states, of the H_2^+ ion for $\Theta=0°$ and in the range $B=0.01$–1.0 in Ref. [30]. The result of this estimation is that the energies due to the mass corrections and, in particular, due to the coupling of the center-of-mass motion and to the internal degrees of freedom are at least two orders of magnitude smaller than the spacing of the electronic energies in the fixed-nuclei approach. Since the order of magnitude of these correction terms is expected to not change significantly if we incline the internuclear axis with respect to the magnetic-field axis, the fixed-nuclei approach is, for the above electronic states and field strengths, a good starting point for an investigation of the electronic PESs of the H_2^+ ion.

In order to specify our working Hamiltonian we locate the two protons in the x-z plane and choose the midpoint of the internuclear axis as the coordinate origin. The magnetic-field vector $\mathbf{B}$ is assumed to point along the z axis. The orientation of the H_2^+ ion relative to the magnetic field is given by the vector $\mathbf{R}=R(\sin\Theta,0,\cos\Theta)^T$, where R represents the internuclear distance. The electronic fixed-nuclei Hamiltonian therefore takes on the form

$$H_{\mathrm{fix}}=-\tfrac{1}{2}\nabla^2+\tfrac{1}{2}BL_z+\tfrac{1}{8}B^2(x^2+y^2)+V(\mathbf{r},\mathbf{R}), \qquad (1)$$

where x,y,z are the components of the position vector $\mathbf{r}$ of the electron and L_z is the projection of the angular momentum onto the magnetic field axis. For the vector potential we have adopted the symmetric gauge $\mathbf{A}(\mathbf{r})=\frac{1}{2}(\mathbf{B}\times\mathbf{r})$. $V(\mathbf{r},\mathbf{R})$ contains all Coulomb interaction terms of the electron and nuclei.

The symmetries of the Hamiltonian (1) depend strongly on the orientation of the internuclear axis with respect to the magnetic field [37]. For the parallel configuration ($\Theta=0°$), both the parity and rotations around the internuclear axis are symmetries. The resulting symmetry point group is the $C_{\infty h}$ group. For the orthogonal configuration ($\Theta=90°$), the parity as well as the z parity are conserved quantities, i.e., we obtain the symmetry point group C_{2h}. In contrast, for the case $0°<\Theta<90°$ the only remaining symmetry is the parity, which corresponds to the symmetry point group C_i. The parallel and orthogonal configurations are therefore distinguished by their higher symmetry. As a consequence of these symmetry properties of the Hamiltonian (1), the PESs of two electronic states with the same parity but different symmetries at $\Theta=0°$ or 90°, i.e., different magnetic quantum number or different z parity, are allowed to cross each other at $\Theta=0°$ or 90°. These crossings turn into avoided crossings if we incline the internuclear axis with respect to its parallel or orthogonal position. Avoided crossings of PESs with the same parity for $0°<\Theta<90°$ are a consequence of the noncrossing rule, which holds for our complex Hermitian eigenvalue problem of the Hamiltonian (1) [38].

The eigenfunctions and corresponding eigenvalues of the Hamiltonian (1) are characterized by the quantum numbers belonging to the different orientations of the molecule with respect to the magnetic field. This means that the eigenfunctions are labeled $n\sigma$ (σ for the magnetic quantum number $m=0$), $n\pi$ (π for $m=-1$), etc., for $\Theta=0°$ and n^+,n^- ($+,-$ for positive- and negative-z parity, respectively) for $\Theta=90°$. The label n represents the degree of excitation within a manifold of a given quantum number at either $\Theta=0°$ or $90°$. An additional subscript g or u (g,u for gerade and ungerade parity, respectively) characterizes the inversion symmetry of the electronic wave functions at $\Theta=0°,90°$. In the case of $0°<\Theta<90°$ the wave functions will be characterized solely by the subscript g or u and the label n.

In order to solve the electronic Schrödinger equation belonging to the fixed-nuclei Hamiltonian (1), we expand the electronic eigenfunctions in terms of nonorthogonal molecular orbitals. These molecular orbitals are built up by the optimized basis set of generalized atomic orbitals, which is a key ingredient for our numerical calculation of the spectrum and eigenfunctions of the H_2^+ ion. For a detailed description of the optimized atomic orbital basis functions, a discussion of the relevance and properties of the nonlinear variational parameters including the gauge phase, and the method of construction of the molecular orbitals we refer the reader to Refs. [27–30]. The resulting generalized eigenvalue problem is solved numerically by using standard techniques.

Finally, a remark on the numerical effort of our calculations is appropriate. In order to obtain the desired accuracy, 10^{-3}–10^{-4} of the energy eigenvalues, we had to use a basis set of 300–400 atomic orbital functions, depending on the angle of the internuclear with respect to the magnetic-field axis. The average CPU time to get one point, i.e., for one configuration (R,Θ), using a Silicon Graphics Indigo R4000 workstation, was between 6 and 12 h, depending on the number of basis functions. The total CPU time of our investigation, therefore, amounts to more than 2 yr on the above computer.

III. THE ORTHOGONAL CONFIGURATION: ELECTRONIC STATES WITH POSITIVE-z PARITY

The orthogonal configuration of the H_2^+ ion in a strong magnetic field is, as we mentioned above, distinguished by its high symmetry. The conserved quantities are the parity P and the z parity π. In the presence of a magnetic field $B=1.0$ the energetically low-lying molecular electronic states possess positive-z parity. The corresponding electronic states with negative-z parity possess a node along the z direction and belong to a higher degree of excitation in energy. This statement holds for the subspaces with gerade and ungerade parity. We focus in the present section on the six lowest electronic states in each of the subspaces with gerade and ungerade parity. These electronic states are exclusively states with positive-z parity.

Before we start our investigation of the molecular states for $\Theta=90°$, let us comment on some properties of the molecular orbitals used to build up the electronic fixed-nuclei wave functions. In general, the molecular orbitals are chosen as eigenfunctions of the parity operator P and the z component of the angular momentum operator L_z. For the special case of the parallel configuration a particular electronic wave function with a given magnetic quantum number m and parity P is expanded solely in terms of molecular orbitals with the same magnetic quantum number m and parity P [30]. If we incline the internuclear axis with respect to its parallel position, we obtain a strong symmetry lowering. The corresponding electronic wave functions for $\Theta\neq0°$ are then built up from molecular orbitals belonging to different magnetic quantum numbers m, i.e., we obtain a so-called m mixing in the decomposition of the electronic wave functions into molecular orbitals. As a consequence, a substantial increase in the size of the basis set is necessary for $\Theta\neq0°$ in order to obtain the same accuracy with respect to energy as for the case $\Theta=0°$. For a fixed magnetic-field strength, this m mixing depends strongly on the orientation of the internuclear axis with respect to the magnetic-field axis, on the internuclear distance R, and the degree of excitation n.

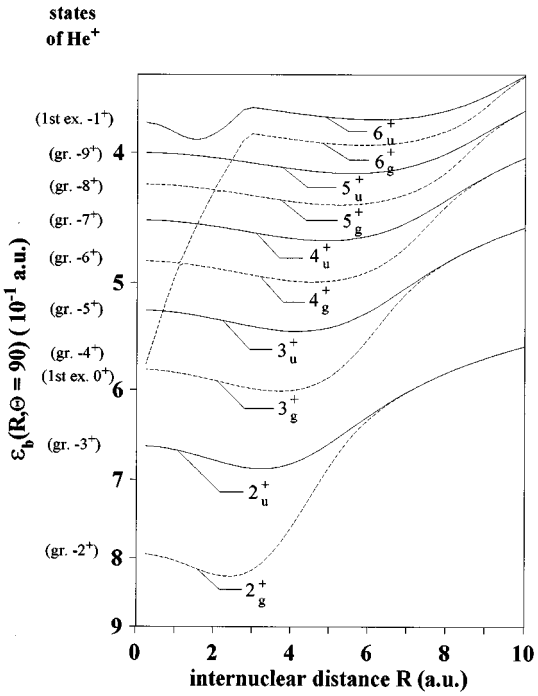

FIG. 1. Molecular orbital correlation diagram for the six lowest gerade and ungerade electronic states with positive-z parity for $\Theta=90°$. The united atom He^+ states are also indicated.

In the following subsection we consider the correlation diagrams between the united atom $R\rightarrow0$ limit and the separated atom $R\rightarrow\infty$ limit at $\Theta=90°$. This will later on yield information on the contribution of molecular orbitals with different magnetic quantum numbers m to a certain molecular electronic state.

A. The molecular-orbital correlation diagram at $\Theta=90°$

Figure 1 shows the electronic orbital binding energies $\epsilon_b(R)$ as a function of the internuclear distance R at $\Theta=90°$ for the first five excited states of each subspace with gerade and ungerade parity for $B=1.0$. Since the orbital binding energy curves of the ground states 1_g^+ and 1_u^+ are energetically well separated from all other curves belonging to the electronic states with positive-z parity, they have been omitted in Fig. 1. The energy $\epsilon_b(R)$ does not include the inter-

nuclear repulsion but the threshold energy $\epsilon_{\rm th}$, which shifts the ionization threshold to zero energy, i.e., $\epsilon_b(R)=\epsilon_{\rm th}-\epsilon(R)+1/R$, where $\epsilon(R)$ is the electronic energy belonging to the Hamiltonian (1). The threshold energy for an arbitrary molecular state of the H_2^+ ion is given by the lowest energy of a free electron, i.e., by the energy of the lowest Landau level $\epsilon_{\rm th}=B/2$.

It can be easily seen that the parity P and z parity π for a molecular electronic state for a finite internuclear distance turn, in the limit $R\rightarrow 0$, into the parity and z parity of the united atom, respectively. For the considered molecular states with positive-z parity this means that the united-atom electronic He^+ states possess positive-z parity as well. Since the parity of hydrogenlike atoms is given by the relation $(-)^P=(-)^{\pi}(-)^m$, the corresponding molecular states with gerade parity will, for $R\rightarrow 0$, turn into He^+ states with even magnetic quantum numbers, while the molecular states with ungerade parity will turn into He^+ states with odd magnetic quantum numbers. These are general properties of the correlation between the molecular states at $\Theta=90°$ and the united-atom states.

In order to completely specify the united-atom limit of a particular molecular electronic state it is necessary to know the order of energies of the He^+ states for the relevant subspace $(P\pi)$. This order, however, depends sensitively on the applied magnetic-field strength. For example, in Fig. 1, for $B=1.0$ we observe that for $R\rightarrow 0$ the 2_g^+ molecular state becomes the ground state of the atomic He^+ subspace $m=-2^+$. The 3_g^+ molecular state turns, for $R\rightarrow 0$, into the first excited state of the He^+ subspace $m=0^+$. The reason for this behavior is the fact that the first excited state of the subspace $m=0^+$ of the He^+ atom is energetically lower than the He^+ ground state of the subspace $m=-4^+$. In the case of a strong change of the magnetic-field strength, the above-mentioned order of energies might be changed significantly or even completely reversed. In particular, for one-electron atoms it has been shown in the literature [39] that the ground states of the subspaces with positive-z parity become infinitely strongly bound in the limit $B\rightarrow\infty$.

Figure 1 shows us also the behavior of the magnetically dressed molecular states for $\Theta=90°$ at large internuclear distances. In the separated-atom limit $(R\rightarrow\infty)$, each pair of the g-u states becomes degenerate, i.e., the gerade and ungerade molecular states change for $(R\rightarrow\infty)$ into the same separated-atom state of the hydrogen atom. Since the z parity is conserved for the orthogonal configuration, the separated-atom state and the corresponding molecular state for finite internuclear distance possess, independently of their parity, the same z parity.

Into which separated atom state a given g-u pair of magnetically dressed electronic states changes for $R\rightarrow\infty$ depends now on the order of energies of the states of the hydrogen atom. The latter varies for a given z parity with the strength of the external magnetic field. In our case with $B=1.0$, the $2_{g/u}^+,\ldots,6_{g/u}^+$ molecular states turn, for $R\rightarrow\infty$, into the lowest, i.e., ground states, of the hydrogen atom with magnetic quantum numbers $m=-1,\ldots,-5$ and positive-z parity, respectively.

Figure 2 shows the total electronic energy curves $\epsilon_T(R)=\epsilon(R)-\epsilon_{\rm th}$ for the same electronic states of the H_2^+ ion for which the electronic orbital binding energy curves have been presented in Fig. 1. We observe that two molecular states with the same degree of excitation and the same z parity, but gerade and ungerade parity, represent a pair of so-called ''bonding'' and ''antibonding'' states, respectively. The electronic states can therefore be grouped in the bonding $2_g^+,3_g^+,\ldots$ states and the antibonding $2_u^+,3_u^+,\ldots$ states. Each of the potential-energy curves of the gerade magnetically-dressed molecular states exhibits a well-pronounced potential well. The potential-energy curves of the corresponding ungerade states exhibit only flat potential wells (a detailed discussion of the stability of the considered states with respect to dissociation is given in Sec. III C). With increasing internuclear distance R, the g-u splitting of the energy curves for a given degree of excitation reduces rapidly.

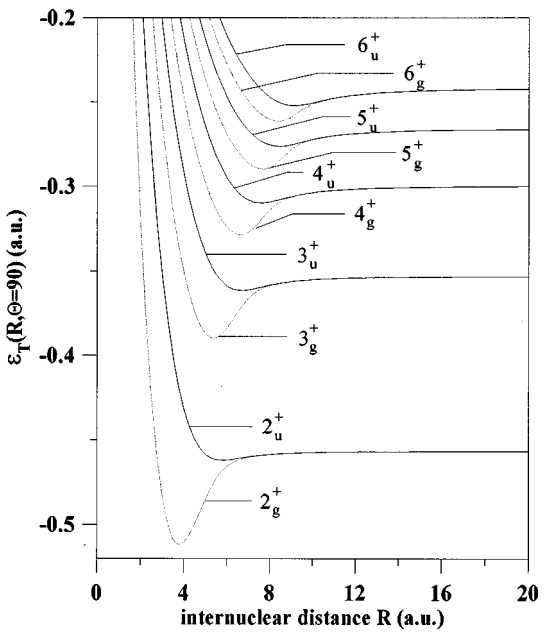

FIG. 2. Adiabatic potential-energy curves of the five lowest excited gerade and ungerade electronic states with positive-z parity for $\Theta=90°$. The separated atom H states are also indicated.

B. m-mixing properties

After having discussed the molecular-orbital correlation diagrams for electronic states with positive-z parity, we are now in the position to give an answer to the question raised at the beginning of the present section: what are the magnetic quantum numbers of the molecular orbitals that provide a relevant contribution to the molecular electronic wave function for a given nuclear configuration and field strength? The magnetic quantum number m of the united-atom state arising from a certain molecular state in the limit $R\rightarrow 0$ increases, in general, more rapidly than the degree of excitation of the underlying molecular state. For instance, as $R\rightarrow 0$, the $3_u^+,4_u^+,5_u^+$ molecular states change into the lowest He^+ states with the magnetic numbers $m=-5,-7,-9$ and positive-z parity, respectively. For decreasing internuclear distances the contribution of the molecular orbitals with magnetic quantum numbers higher than the degree of energetic excitation of the considered molecular state increases rapidly. For example, in order to achieve an accuracy of $\sim 0.1\%$ in energy for the 5_u^+ molecular state for internuclear

distances ($R \leqslant 4$), we have to build up the corresponding electronic molecular wave function from orbitals characterized by magnetic quantum numbers up to $|m|=9$. In contrast to this the magnetic quantum number m of a separated-atom state, which evolves from a certain g-u pair of molecular states in the limit $R \rightarrow \infty$, is, in regard to its absolute value, comparable to the degree of excitation n of the corresponding g-u pair of molecular states. This means that for large internuclear distances the important contributions to, for example, the 5_u^+ state come from the molecular orbitals with the magnetic quantum numbers $|m| \leqslant 4$. To summarize, the molecular orbitals that provide the most important contributions to the molecular wave function belong, for small internuclear distances, to much higher magnetic quantum numbers than for large internuclear distances, i.e., the m mixing is particularly strong for small internuclear distances.

For the basis-set calculations of the molecular states with gerade z parity at $\Theta=90°$, the results of which will be discussed in the following subsection, molecular orbitals with magnetic quantum numbers up to $|m|=10$ have been included. In total we used a basis set of 298 optimized atomic orbital functions. This basis-set results for the whole range of internuclear distances in an overall accuracy of significantly less than 0.1% for the $1_{g/u}^+,\ldots,5_{g/u}^+$ states and an accuracy of approximately 0.1% for the $6_{g/u}^+$ states.

C. Adiabatic potential-energy curves for the orthogonal configuration and their binding properties

In the present subsection we discuss the binding properties of the $1_{g/u}^+,\ldots,6_{g/u}^+$ magnetically dressed states that belong to the orthogonal configuration for $B=1.0$. With the exception of the potential-energy curves of the $1_{g/u}^+$ molecular states, the corresponding energy curves are displayed in Fig. 2. As already mentioned in Sec. III A, we observe from Fig. 2 that all potential-energy curves of the gerade molecular states exhibit well-pronounced potential wells. The depth of these wells, i.e., the dissociation energies ϵ_D, decrease with increasing degree of excitation n. For example, the dissociation energy of the 1_g^+ state is 1.191×10^{-1}, while the dissociation energy of the 6_g^+ state is 1.941×10^{-2}. A complete list of the dissociation energies as well as the equilibrium internuclear distances is given in Table I. The potential-energy curves of the corresponding ungerade molecular states also exhibit potential wells. The depths of these wells is in each case much less than the depths of the wells of the corresponding gerade states. However, the dissociation energies of the ungerade states increase with increasing degree of excitation (see Table I). For instance, the dissociation energy of the 1_u^+ state is 2.685×10^{-4}, whereas the dissociation energy of the 6_u^+ state is 1.002×10^{-2}.

The existence of a potential well in the adiabatic electronic potential-energy curve is a necessary, but not a sufficient, condition for the formation of a stable molecular bond. In addition, we have to show the existence of vibrational states in the potential wells of the magnetically dressed $1_{g/u}^+,\ldots,6_{g/u}^+$ states considered. To this end we perform a harmonic approximation of the corresponding potential wells around their minima and estimate the ground-state energies of the vibrational states in these harmonic potential wells under the influence of an external magnetic field. As a rough estimate, an upper limit of the energy of the vibrational ground states for the H_2^+ ion is then given by the sum of the ground-state energy in the harmonic potential and the corresponding zero-point cyclotron energy. The zero-point cyclotron energy is, for $B=1.0$, approximately 7.4×10^{-4}. The depth of the potential well of the 1_u^+ state is much smaller than the zero-point cyclotron energy. This state is therefore supposed to be unbound. For all other states, i.e., the $1_g^+,2_{g/u}^+,\ldots,6_{g/u}^+$ states we obtain harmonic vibrational ground-state energies that are roughly one order of magnitude smaller than the corresponding depths of the potential wells. The estimated vibrational ground-state energies for the nuclear motion in each adiabatic potential-energy curve of the $1_g^+,2_{g/u}^+,\ldots,6_{g/u}^+$ states is therefore much smaller than the corresponding dissociation energies. Hence vibrational states do exist in the wells of the potential-energy curves of the $1_g^+,2_{g/u}^+,\ldots,6_{g/u}^+$ states, i.e., these states are stable for the fixed orthogonal configuration (see below).

TABLE I. Equilibrium internuclear distances, total electronic energies, and dissociation energies for the six lowest gerade and ungerade electronic states with positive-z parity for $\Theta=90°$.

State	R_{eq} (in a.u.)	$\epsilon_T(R_{\mathrm{eq}})$ (in a.u.)	ϵ_D (in a.u.)
1_g^+	1.65	-9.4887×10^{-1}	1.191×10^{-1}
2_g^+	3.79	-5.1195×10^{-1}	5.540×10^{-2}
3_g^+	5.37	-3.8993×10^{-1}	3.689×10^{-2}
4_g^+	6.62	-3.2856×10^{-1}	2.859×10^{-2}
5_g^+	7.66	-2.8995×10^{-1}	2.377×10^{-2}
6_g^+	8.39	-2.6159×10^{-1}	1.941×10^{-2}
1_u^+	5.45	-8.2999×10^{-1}	2.685×10^{-4}
2_u^+	5.78	-4.6183×10^{-1}	5.278×10^{-3}
3_u^+	6.67	-3.6138×10^{-1}	8.338×10^{-3}
4_u^+	7.57	-3.0964×10^{-1}	9.678×10^{-3}
5_u^+	8.41	-2.7637×10^{-1}	1.018×10^{-2}
6_u^+	9.15	-2.5222×10^{-1}	1.002×10^{-2}

However, since the angle Θ between the internuclear and magnetic field axes is an additional degree of freedom with, depending on the field strength, rotational-vibrational character, we have to take into account this degree of freedom in order to investigate the global binding properties of the above-discussed states. This means we have to study the topology of the corresponding adiabatic electronic PESs $\epsilon_T(R,\theta)$. In the following section we present and discuss the results of our extensive investigations on the topological properties of the PESs of the $1_{g/u}$, $2_{g/u}$, and $3_{g/u}$ adiabatic electronic states. The PESs of the $4_{g/u}$, $5_{g/u}$, and $6_{g/u}$ states show a much more complicated behavior and will be discussed elsewhere.

IV. ADIABATIC ELECTRONIC STATES AND THEIR POTENTIAL-ENERGY SURFACES FOR ARBITRARY ANGLE Θ

The parity P is the only symmetry for arbitrary orientations of the internuclear axis of the H_2^+ ion with respect to the magnetic field. Since the parallel and orthogonal configu-

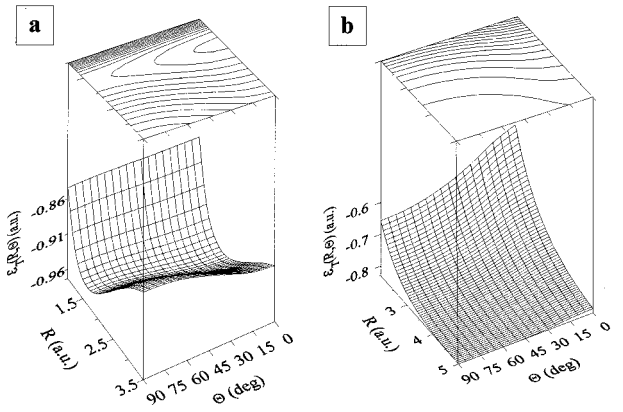

FIG. 3. Potential-energy surfaces of the ground states with (a) gerade parity, i.e., the 1_g electronic state, and (b) ungerade parity, i.e., the 1_u electronic state, shown together with their contour plots.

rations are distinguished by their higher symmetries, the PESs of two electronic states of a given subspace P, i.e., of the same parity but different symmetries at $\Theta=0°$ and/or $\Theta=90°$, are allowed to cross each other without interacting at these positions. These crossings turn into avoided crossings if we incline the internuclear axis away from the parallel or orthogonal position. As a result, the common manifold of intersecting PESs is a conical intersection point. The potential-energy curves $\{\epsilon_T(R)\}$ arising from a section through a given PES nP at $\Theta=0°$ or 90° can therefore, in general, belong to electronic states with different spatial symmetries but the same parity. Hence the correlation between electronic states at $\Theta=0°$ and those at $\Theta=90°$ via an adiabatic PES depends strongly on the internuclear distance R.

The behavior of diabatic potential energies in the vicinity of $\Theta=0°$ and 90° is due to the higher symmetry of these configurations of special interest and has been investigated for diatomic molecules in Ref. [37]. By using the Hellmann–Feynman theorem and the respective symmetries at $\Theta=0°$ and 90°, it was shown that the diabatic energies possess extreme at these distinct positions. From these results one might conjecture that for low-lying electronic states either the parallel or the orthogonal configuration represents the global, i.e., energetically lowest, equilibrium configuration of the corresponding surfaces. For instance, the PES of the well-known ground state of the H_2^+ ion in a strong magnetic field exhibits its global equilibrium configuration at $\Theta=0°$ [13–16]. In addition, it was shown in Ref. [16] that there exist excited electronic states that have at least a local potential minimum at $\Theta=90°$. However, until now it had been an open question what the global topology of the PES of the excited electronic states of the H_2^+ ion in a strong magnetic field looks like and in particular how it evolves with increasing degree of excitation. In the following section we will investigate the local as well as global topological properties of the three lowest PESs with gerade and ungerade parity.

A. PESs of the 1_g and 1_u states

Let us first consider the PESs of the lowest electronic states with gerade and ungerade parity. In Fig. 3(a) the two-dimensional energy surface of the 1_g state, i.e., the ground state, of the H_2^+ ion, together with the corresponding contour plot, is displayed for a magnetic-field strength $B=1.0$. The potential-energy curve that results from the section through the 1_g PES at $\Theta=0°$ belongs to the $1\sigma_g$ state and the section taken at $\Theta=90°$ belongs to the 1_g^+ state. The $1\sigma_g$ and the 1_g^+ states are energetically well separated from all other electronic states with equal symmetries, respectively. We encounter, therefore, a one-to-one correlation of the $1\sigma_g$ state at $\Theta=0°$ to the 1_g^+ state at $\Theta=90°$ via the adiabatic 1_g PES for arbitrary internuclear distance R. In particular, the 1_g state does not interact vibronically with the electronically excited states. The equilibrium configuration of the 1_g PES, i.e., the global minimum of the PES, occurs at $\Theta=0°$ and $R_{\rm eq}^0=1.76$. The corresponding depth of the potential well, i.e., the dissociation energy ϵ_D^0, for the parallel configuration is 1.437×10^{-1} [28]. If we incline the internuclear axis with respect to the magnetic field, the dissociation energy ϵ_D^Θ, as well as the ''equilibrium'' internuclear distance $R_{\rm eq}^\Theta$, decreases. At $\Theta=90°$ we find a dissociation energy $\epsilon_D^{90°}=1.191\times10^{-1}$ and an equilibrium internuclear distance $R_{\rm eq}^{90}=1.65$ (see Table I). We note that our values $R_{\rm eq}^0$ and $R_{\rm eq}^{90}$ for $B=1.0$ are in very good agreement with the corresponding values found by Larsen [13] and Wille [16].

Since the energy difference between the dissociation energies of the parallel and orthogonal configurations is only of the order of magnitude 10^{-2}, it is not clear *a priori* whether the shallow potential barrier in the direction of the angle Θ can, for the lowest rovibrational states, prevent the H_2^+ ion from rotational motion in the angle Θ. In order to decide this we have to estimate the energy of the lowest vibrational states in the well of the 1_g PES. To this end we approximate the two-dimensional potential well by a harmonic potential and estimate the ground-state energy of the nuclear motion in this harmonic potential under the influence of the external magnetic field. An upper limit of the energy of the vibrational ground state is then given by the sum of the ground-state energies of the harmonic vibrations parallel ($\frac{1}{2}\omega_R$) and perpendicular ($\frac{1}{2}\omega_\Theta$) to the magnetic field around the global equilibrium position ($R_{\rm eq}^0$,0°) and the corresponding zero-point cyclotron energy. For the 1_g state considered with $B=1.0$, we obtain a harmonic potential ground-state energy of the order of magnitude of 1×10^{-2}. This vibrational ground-state energy is approximately half the height of the potential barrier in the direction of the angle Θ, which is $\Delta\epsilon=\epsilon_D^0-\epsilon_D^{90}=2.43\times10^{-2}$. In addition, the estimated level spacing of the harmonic vibration of the Θ mode ω_Θ is of the order of magnitude 10^{-4}. As a consequence, many vibrational states exist in the shallow two-dimensional potential well of the 1_g state. Rotational motion in the angle Θ is, therefore, for the low-lying vibrational states possible only via a tunneling process through the potential barrier. The estimated level spacing of the vibrational motion in R is of the order of magnitude of 2×10^{-2}. Hence vibrationally excited states belonging to the totally symmetric mode R are not prevented from free rotation in the angle Θ.

Let us now consider the lowest PES of the H_2^+ ion with ungerade parity, i.e., the 1_u state, which is illustrated together with the corresponding contour plot in Fig. 3(b). The two potential-energy curves obtained by the sections through the 1_u PES at $\Theta=0°$ and 90° belong to the $1\sigma_u$ and 1_u^+ electronic states of the parallel and orthogonal configurations, respec-

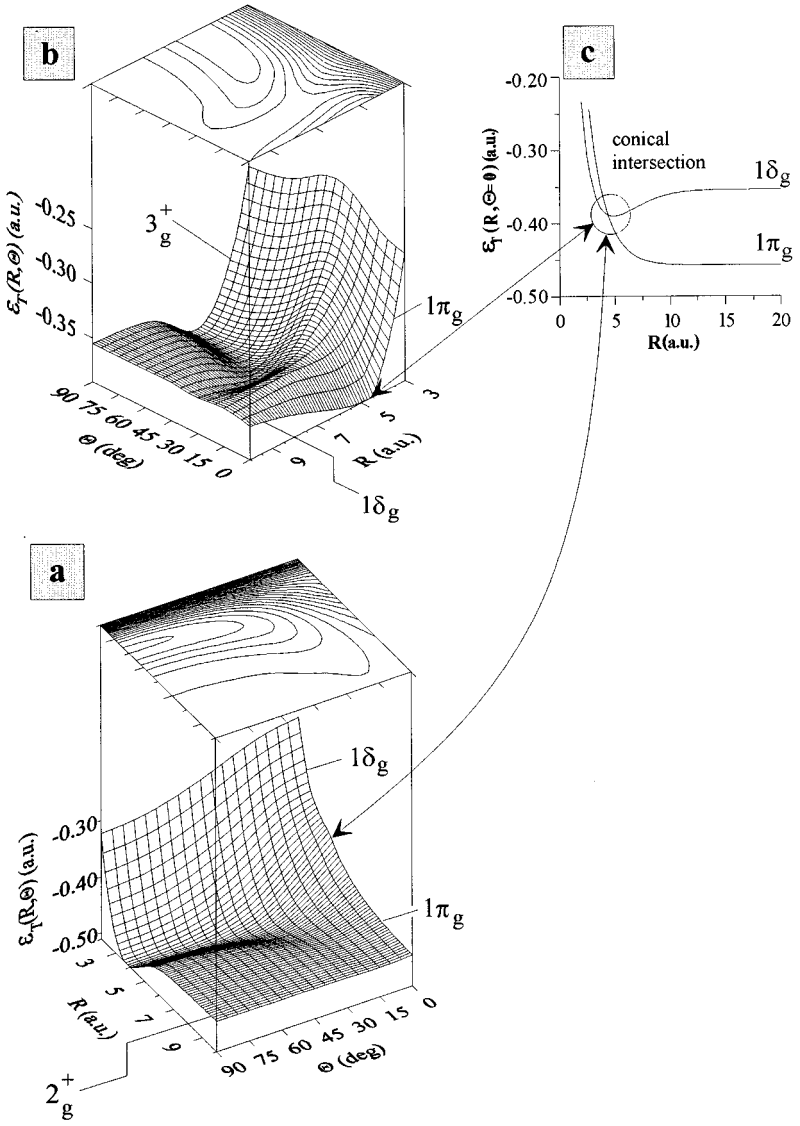

FIG. 4. Potential-energy surfaces of the (a) 2_g state and (b) 3_g state shown together with their contour plots. In (c) the conical intersection of the $1\pi_g$ and $1\delta_g$ states at $\Theta=0°$ is illustrated.

tively. For the 1_u PES we encounter a conical intersection point with the upper 2_u state at $\Theta=0°$ and $R\approx1.6$ (cf. the discussion of the 2_u state in Sec. IV C). Since this intersection point occurs in the strongly repulsive part of the 1_u PES, it is irrelevant for the bonding properties of this state. Apart from this conical intersection point, the PES of the 1_u state is energetically well separated from the PES of all other electronic states with ungerade parity.

The PES of the 1_u state exhibits a very shallow potential well; for the parallel configuration we obtain an equilibrium distance of $R_{\rm eq}^0=9.6$ and a dissociation energy $\epsilon_D^0=2.7\times10^{-4}$, while the equilibrium distance at $\Theta=90°$ is $R_{\rm eq}^{90}=5.45$ and the dissociation energy has, within our computational accuracy, the same value as for $\Theta=0°$ (cf. Table I). Since the depth of the corresponding two-dimensional potential well is much smaller than the zero-point cyclotron energy of the nuclear motion (see Sec. III C) the 1_u state is supposed to be unbound.

The simple topological properties of the $1_{g/u}$ PES of the H_2^+ ion for $B=1.0$ have their origin in the minor changes of the shape of the corresponding electronic density distributions with varying angle Θ [16]. However, as we shall see in the following subsections, the density distributions of the excited states depend strongly on the angle Θ and therefore the topology of the corresponding PES is much more complex.

B. The lowest excited states with gerade parity

1. PESs of the 2_g and 3_g states

In Figs. 4(a) and 4(b) the PESs of the 2_g and 3_g state are illustrated, together with their respective corresponding contour plots. Let us first consider the PES of the 2_g state [see Fig. 4(a)]. It possesses a single, and hence global, minimum at $\Theta=90°$. The potential-energy curve that results from the section through the 2_g PES at $\Theta=90°$ belongs to the excited 2_g^+ state, which has been discussed in Sec. III. The equilibrium configuration and the depth of the two-dimensional potential well are therefore identical to the data we obtained for the 2_g^+ state, i.e., $R_{\rm eq}^{90}=3.79$ and $\epsilon_D^{90}=5.54\times10^{-2}$ (cf. Table I).

Analogous to the case of the 1_g state, the two-dimensional potential well of the 2_g state is well pronounced in the direction of the internuclear distance R, but much flatter in the angle Θ. However, compared to the ground state of the H_2^+ ion, the potential barrier in the rotational degree of freedom

Θ is much higher. This is due to the strongly repulsive behavior of the 2_g PES in the vicinity of $\Theta=0°$, where the potential energies for arbitrary internuclear distances lie above the energy threshold for dissociation. Hence rotation of the H_2^+ ion in the 2_g state for $B=1.0$ via a tunneling process is strongly suppressed. In order to estimate whether vibrational states exist in the two-dimensional potential well, we again follow the procedure described in Sec. IV A. The corresponding estimation proves the existence of a large number of vibrational states in this well, i.e., the 2_g state is a stable molecular state with its global equilibrium configuration at $\Theta=90°$.

Let us now briefly consider the potential-energy curve defined by the section through the 2_g PES at $\Theta=0°$. It consists of two parts: the upper part belongs to the $1\delta_g$ state and the lower part to the $1\pi_g$ state. Due to their different symmetries the $1\delta_g$ and $1\pi_g$ states are allowed to cross each other at $R\approx4.5$ [see Fig. 4(c)]. From the point of view of the PES, we encounter a conical intersection of the lower 2_g and the upper 3_g PES. In the vicinity of this intersection point vibronic coupling effects are important and the 2_g and 3_g states are strongly coupled via the nuclear motion. However, the effect of this vibronic coupling is, due to the location of the conical intersection point in the strongly repulsive part of the 2_g PES, of no relevance for the binding properties of the 2_g state.

For the binding properties of the 3_g state, whose PES meets the 2_g PES at the above-mentioned conical intersection point, the vibronic coupling effects play, as we shall see shortly, an important role. Similar to the 2_g PES, the 3_g PES [see Fig. 4(b)], which will be discussed in the remaining part of this subsection, possesses its global minimum at $\Theta=90°$. However, this potential well is separated by a potential barrier from a second minimum at $\Theta=0°$. The depths of both potential wells, i.e., the dissociation energies, are almost equal ($\epsilon_D^0=3.641\times10^{-2}$, $\epsilon_D^{90}=3.689\times10^{-2}$), while the corresponding equilibrium internuclear distances differ by 0.5 ($R_{\rm eq}^0=4.87$ and $R_{\rm eq}^{90}=5.37$). In spite of the minimum of the 3_g PES at $\Theta=0°$, the parallel configuration cannot be considered as stable since the conical intersection with the lower 2_g PES is very close to the minimum of the well of the 3_g PES at $\Theta=0°$ [cf. Fig. 4(c)]. Vibronic interaction is therefore important close to the bottom of the well at $\Theta=0°$ and causes a strong mixing of the electronic and nuclear wave functions. A wave packet originally located on the upper 3_g surface will rapidly decay to the lower 2_g surface, followed by the dissociation process of the molecule.

In contrast to the potential well around the parallel configuration, the well with the global minimum around $\Theta=90°$ is energetically well separated from all other states with the same symmetries. Again an estimation shows that many vibrational states exist in the well of the 3_g PES located at $\Theta=90°$, i.e., the orthogonal configuration of the 3_g state is a stable molecular state. In order to gain more insight and enhance our understanding of the origin of the above-described topological behavior of the PESs of the 2_g and 3_g states, we consider in the following, the electronic probability density distributions for both states as a function of the angle Θ.

2. Electronic density distributions

In Figs. 5(a) and 5(b) the electronic probability densities for the 2_g and the 3_g states are shown for several configurations (R,Θ), respectively. The positions of these configurations are indicated on the contour plots of the corresponding 2_g and 3_g PESs, which are also presented in Figs. 5(a) and 5(b), respectively. The internuclear distance R belonging to the illustrated densities of the 2_g state is always the equilibrium distance $R_{\rm eq}^{90}$. The configurations we have chosen in nuclear coordinate space (R,Θ) for studying the densities of the 3_g state lie on the line that connects the minimum at $\Theta=0°$ with the minimum at $\Theta=90°$.

In contrast to the contour plots of the PESs that are given in nuclear coordinate space (R,Θ), the contour plots of the electronic density distributions shown, for example, in Fig. 5 are plotted in the electronic x-z coordinate plane ($y=0$). Since the orientation of the molecule in this plane is given by $R=\sqrt{R_x^2+R_z^2}$ and $\Theta=\arctan(R_x/R_z)$ (cf. Sec. II), the internuclear axis rotates in the x-z plane with varying angle Θ, i.e., for the parallel configuration the internuclear axis points along the z axis ($\|\mathbf{B}$), while for the orthogonal configuration the internuclear axis is aligned with the x axis.

Let us begin our investigation of the electronic density distributions with varying angle Θ by considering Fig. 5(a) I–V for the 2_g state. As already discussed, the global minimum of the 2_g PES occurs at $\Theta=90°$. The corresponding electronic density distribution in Fig. 5(a) V shows a global maximum that is strongly peaked at $x=z=0$, i.e., exactly between both nuclei, which are located at $|x|=1.9$ and $z=0$, respectively. The outer maxima, which are separated by nodes from the global maximum, occur on the internuclear axis at the positions $|x|=2.5$. The value of the global maximum is approximately three times that of the outer maxima. Since the 2_g PES is for $45°<\Theta<90°$ energetically well separated from the PESs of all other states with the same symmetries, vibronic coupling effects are negligible in this regime. The large probability of finding the electron between both nuclei for $\Theta=90°$ leads to a screening for the nuclear charges and a lowering of the potential energy. The formation of the two-dimensional well of the 2_g PES around $\Theta=90°$ has, therefore, its origin in the strong localization of the electronic density in the form of a global maximum between both nuclei.

With decreasing angle Θ [cf. Figs. 5(a) IV for $\Theta=60°$ and 5(a) III for $\Theta=30°$], the absolute value of the inner global maximum decreases rapidly and eventually becomes only a local maximum. The potential energy thereby increases strongly according to the contour plot of Fig. 5(a). Furthermore, as the angle Θ decreases the line connecting the three maxima of the electronic density become more inclined with respect to the x axis. For $\Theta=15°$ the two global maxima of the density are located at $|x|=|z|=1.9$, whereas the positions of the nuclei are given by $|x|=0.49$ and $|x|=1.83$. The electronic wave function has, therefore, acquired a strongly perturbed shape in the sense that the positions of the maxima deviate strongly from the positions of the nuclei and are, in particular, not located on the internuclear axis.

With further decreasing angle Θ, the inner local maximum decreases further and eventually disappears for $\Theta=0°$ [see Fig. 5(a) I, which is taken for $R_{\rm eq}=3.79$]. At $\Theta=0°$ the density peaks due to the outer maxima have become lower but much wider than for other values of the angle Θ. They are located away from the internuclear axis, but with values of the z coordinate that are in between the nuclei. The com-

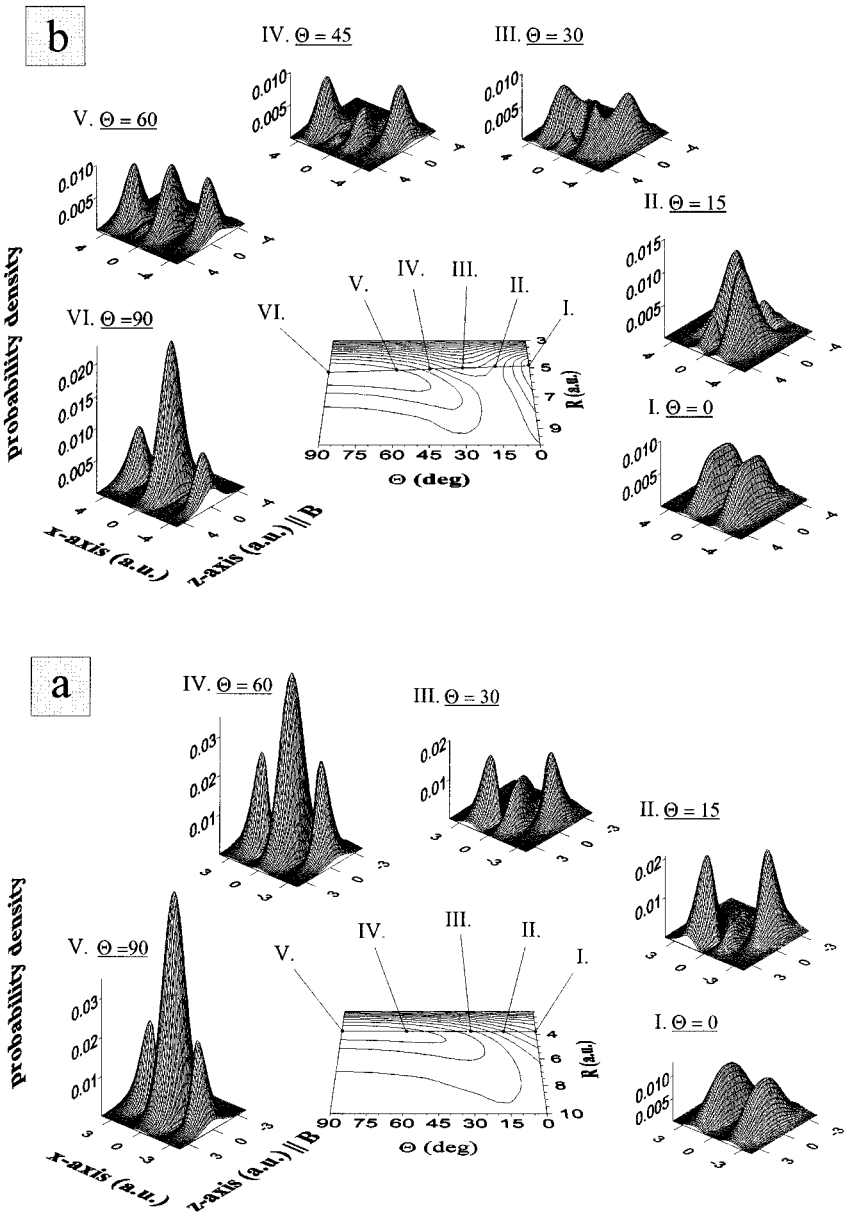

FIG. 5. Contour plots and the electronic probability distributions for selected values (R,Θ) in nuclear configuration space. (a) Contour plot of the PES of the 2_g state and the electronic densities at $\Theta=0°$, 15°, 30°, 60°, and 90°. (b) Contour plot of the PES of the 3_g state and the electronic densities at $\Theta=0°$, 15°, 30°, 45°, 60°, and 90°. (See the indicated points on the straight lines on the individual contour plot.)

ponent of the angular momentum parallel to the magnetic field is now a conserved quantity and the observation that the electronic density is located away from the internuclear axis is a consequence of the finite angular momentum, which is, in our case of Fig. 5(a) I, $|m|=2$ (see below).

The section through the 2_g PES at $\Theta=0°$ belongs not to a single electronic state but to two states with different symmetry. For $R<4.5$ we have the $1\delta_g$ state and for $R>4.5$ the $1\pi_g$ excited electronic state. According to our discussion in Sec. IV B 1, we encounter a conical intersection at $R\approx4.5$. The fact that the electronic density distributions in Fig. 5(a) I is strongly located at values of the z coordinate in between both nuclei suggests an attractive behavior of the potential-energy curve for the $1\delta_g$ state, which is indeed the case. This, however, does not determine the stability properties of the section through the 2_g PES at $\Theta=0°$, which, according to the above discussion, belongs to two different electronic states and results in a purely repulsive potential-energy curve.

In Fig. 5(b) we show the changes of the density distribution of the 3_g state with varying angle Θ and internuclear distance R along the line in (R,Θ) space mentioned above. We begin our investigation with the minimum of the 3_g PES at $\Theta=0°$, which is identical to the equilibrium position of the $1\delta_g$ state. The observed density distribution in Fig. 5(b) I is almost identical to that of the 2_g surface shown in Fig. 5(a) I. The intersection of the 3_g surface at $\Theta=0°$ consists of two electronic states with different symmetries: namely, the repulsive part for $R<4.5$ is due to the $1\pi_g$ state and the attractive part for $R>4.5$ is due to the $1\delta_g$ state. The density distribution at $\Theta=0°$ reflects the attractive behavior of the potential-energy curve of the $1\delta_g$ state, but, due to vibronic coupling effects (see the discussion above), this does not determine the stability properties of the position $\Theta=0°$ on the 3_g surface. If we now incline the internuclear axis with respect to the magnetic-field direction, the potential energy increases strongly [see the contour plot of Fig. 5(b)]. This fact is reflected in the corresponding density distribution; both maxima become more and more peaked and are shifted towards the positions of the individual nuclei. In addition, the maxima are connected via a ridge, i.e., we observe a

saddle point between both nuclei. A snapshot of this redistribution of the density is given in Fig. 5(b) II for $\Theta=15°$. The ridge that connects both global maxima is in Fig. 5(b) II hidden by the corresponding peak in front. We also observe two small additional local maxima, each located close to the position of the individual nucleus. This redistribution of the density of the 3_g state in the region of small values of the angle Θ ($0°<\Theta<25°$) leads to a strongly enhanced probability of finding the electron close to the nuclei. The probability density between both nuclei is, however, very small. This decrease of the probability of finding the electron in the region between both nuclei leads to a weak screening of the nuclear charges and, consequently, to the formation of the observed potential barrier.

After crossing the potential ridge of the 3_g PES we observe a rapidly growing density between both nuclei; the ridge of the electronic density distribution that has connected the two global maxima at $\Theta=15°$ becomes more and more pronounced and, in particular, the saddle point on the ridge that we have observed at $\Theta=15°$ [cf. Fig. 5(b) II] is now changing into an additional local maximum. Both small local maxima that are located close to the nuclei decrease with increasing angle Θ. These features are illustrated in Fig. 5(b) III, where we have plotted the density distribution of the 3_g state at $\Theta=30°$.

Increasing angle Θ further, the density ridge that connects the newly formed local maximum between both nuclei with the global maxima vanishes. We consequently observe the formation of nodes that separate the local inner maximum from the outer global maxima [see Fig. 5(b) IV for $\Theta=45°$]. In addition, the value of the inner local maximum increases more and more with increasing angle Θ and eventually becomes the global maximum of the density [see Fig. 5(b) V]. At $\Theta=90°$ the value of the inner global maximum is two times the values of the outer maxima [cf. Fig. 5(b) VI]. The global maximum is now separated by nodes from the outer maxima. In addition, the two small local maxima, each located close to an individual nucleus for $\Theta<90°$, for the orthogonal configuration have now disappeared. The three remaining maxima at the orthogonal configuration are, similar to the case of the three density maxima of the 2_g state at $\Theta=90°$, located on the x axis; the inner global maximum is centered at the origin while the outer local maxima are located at $|x|\approx 4.0$ and $|z|=0$. In comparison with the density distribution of the 2_g state at $\Theta=90°$, the obtained probability density of the 3_g state for the orthogonal configuration is more widely distributed. Since the 3_g state is, for $\Theta>30°$, energetically well separated from all other PESs with the same symmetry, the observed strong electronic density maximum between both nuclei explains the formation of the two-dimensional potential well of the 3_g PES around its orthogonal equilibrium configuration.

C. Lowest excited states with ungerade parity

We turn now to the discussion of the lowest excited states with ungerade parity. Analogous to the preceding subsection, we first consider the PESs themselves and subsequently explain the topological properties of the 2_u and 3_u PESs by investigating the corresponding density distributions with varying angle Θ.

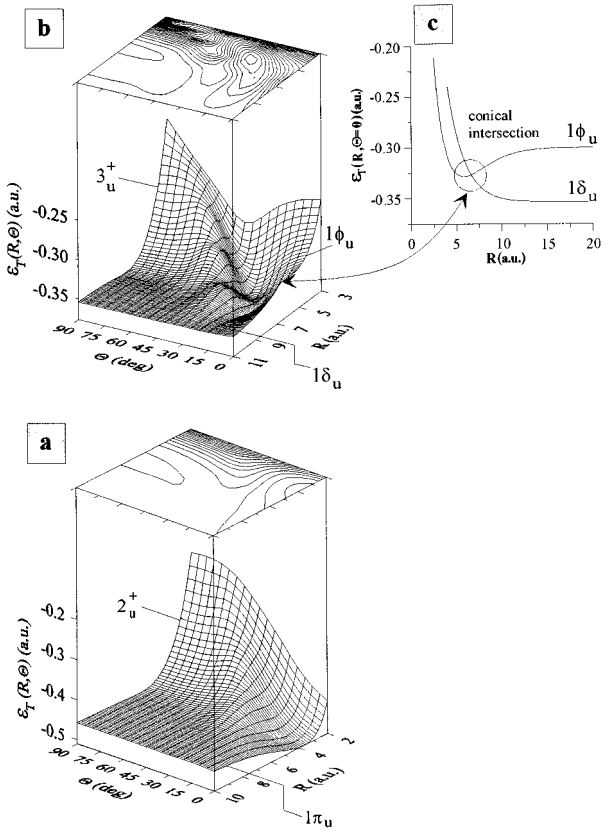

FIG. 6. Potential-energy surfaces of the (a) 2_u state and (b) 3_u state shown together with their contour plots. In (c) the conical intersection of the $1\delta_u$ and $1\phi_u$ states at $\Theta=0°$ is illustrated.

1. PESs of the 2_u and 3_u states

In Fig. 6(a) the PES of the 2_u state is shown together with the corresponding contour plot for a field strength $B=1.0$. The potential-energy curves that result from the sections through the 2_u PES at $\Theta=0°$ and 90° belong to the excited $1\pi_u$ and 2_u^+ states, respectively. The 2_u PES exhibits two potential wells with minima at ($R_{\rm eq}^0=3.68$, $\Theta=0°$) and ($R_{\rm eq}^{90}=5.78$, $\Theta=90°$), respectively. Both potential wells are separated by a potential barrier. The global minimum of the 2_u PES, located at $\Theta=0°$, corresponds to the minimum of the $1\pi_u$ state for the parallel configuration. Hence the depth of the potential well around the parallel configuration is given by the dissociation energy of the $1\pi_u$ state, i.e., $\epsilon_D^0=5.354\times10^{-2}$. In comparison with the shallow potential well at the orthogonal configuration, the potential well around the parallel configuration is much more pronounced; the depth of the potential well at $\Theta=90°$ is $\epsilon_D^{90}=5.278\times10^{-3}$. A rough estimation of the spacing of the vibrational states of the nuclear motion in each potential well shows that there exist a large number of vibrational states in the potential well for the parallel, as well as for the orthogonal configuration. Since the 2_u PES is energetically well separated from all other PESs within our considered range of nuclear coordinate space [see Fig. 6(a)], the 2_u state possesses two stable molecular configurations at $\Theta=0°$ and 90°. The conical intersection point of the 2_u PES at $\Theta=0°$ and $R\approx1.6$ with the lower 1_u state occurs in the strongly repulsive part of the 2_u PES and is therefore irrelevant for the dynamics and in particular the bound-state properties in the

potential wells located at $\Theta=0°$ and 90°. The 2_u electronic state is therefore an example for a ''double-well state''; it possesses two stable molecular configurations that correspond to positions of higher symmetry (the parallel and orthogonal configuration) and are separated by a potential barrier.

So far all stable states discussed above, i.e., the 1_g, 2_g, 3_g, and 2_u states, show equilibrium configurations for distinct positions of higher symmetry. This picture changes if we turn to the 3_u state. The PES of the 3_u state, together with its contour plot, is illustrated in Fig. 6(b) for $B=1.0$. The obviously different feature is the existence of a minimum of the PES at $\Theta\neq 0°,90°$. This minimum is also the global minimum and is located at ($R_{\rm eq}^{27}=5.2$, $\Theta=27°$). The corresponding potential well is well pronounced, i.e., the depth of this well is 2.516×10^{-2}. An estimation of the energy levels of the nuclear motion in this well shows that there exist many vibrational states. In addition to the global minimum, the 3_u PES also possesses a local minimum at ($R_{\rm eq}^{90}=6.67$, $\Theta=90°$). Since the corresponding potential well is rather flat ($\epsilon_D^{90}=8.338\times10^{-3}$), it contains significantly fewer vibrational states than the potential well located at the global minimum. Both wells of the 3_u PES are, analogous to the 2_u PES, separated by a potential barrier. However, in contrast to the 2_u PES, the ridge of the barrier of the 3_u PES is the curve in nuclear configuration space where the upper 4_u PES comes closest to the 3_u PES. The section through the 3_u PES at $\Theta=0°$ represents an energy maximum. This section through the 3_u PES consist of two different parts: the upper part belongs to the $1\phi_u$ state whereas the lower part arises from the $1\delta_u$ state [see Fig. 6(c)]. These two states cross each other at the conical intersection point ($R\approx6.7$, $\Theta=0°$) where, from the point of view of the PES, the lower 3_u surface touches the upper 4_u PES. Since this conical intersection is located far into the purely repulsive part of the 3_u PES, it is irrelevant for the binding properties of the 3_u state. The 3_u state is therefore an example for a molecular state with a strong symmetry lowering in its global minimum, i.e., it exhibits the effect of a global symmetry lowering [40].

2. Electronic density distributions of the 2_u and 3_u states

The topological behavior of the PES is essentially determined by the redistribution of the electronic density with varying internuclear distance R and, in particular, angle Θ. In order to gain insight into the behavior of the PESs of the 2_u and the 3_u states we again consider the density distributions of the 2_u and 3_u states at several distinct configurations (R,Θ). The configurations $[(R_i,\Theta_i),\ i=\text{I, II,...,VI}]$ we have chosen for the 2_u state lie on the line that connects the global minimum of the PES at $\Theta=0°$ with the local minimum at $\Theta=90°$ [see the contour plot of the 2_u PES in Fig. 7(a)]. The density distributions of the 3_u state at the chosen configurations $[(R_i,\Theta_i),\ i=\text{I, II,...,VI}]$ lie on the line that passes the global minimum of the corresponding PES at $\Theta=27°$ and the local minimum at $\Theta=90°$ [cf. the contour plot of the 3_u PES in Fig. 7(b)].

We start our investigation of the electronic density with that of the 2_u state, beginning at the equilibrium configuration $\Theta=0°$ and increasing the angle Θ to the equilibrium configuration $\Theta=90°$. Within the considered nuclear coordinate space (R,Θ) [see the contour plot in Fig. 7(a)], the section of the 2_u PES at $\Theta=0°$ belongs, as mentioned above, to the so-called bonding $1\pi_u$ state. The electronic density distribution of the $1\pi_u$ state at its equilibrium position is illustrated in Fig. 7(a) I. It possesses two density crests separated by a node line along the z axis. They are strongly peaked in the x direction, which corresponds to the direction perpendicular to the magnetic field. Each of the two crests exhibits two maxima at approximately $|x|\approx1.0$ and $|z|\approx1.25$. Between both maxima of a given density crest, the electronic density shows only a very minor decrease. Since the positions of the nuclei are at $|x|\approx1.84$ and $z=0.0$, the large probability of finding the electron in the region close to the internuclear axis for z values between both nuclei leads to an efficient screening of the nuclear charges and is responsible for the formation of the well-pronounced potential well observed. If we now incline the internuclear axis with respect to the magnetic field we have, from the point of view of the 2_u PES, to climb up the potential barrier towards its ridge. The increase of energy along the corresponding path, which is indicated in the contour plot of Fig. 7(a), from the parallel configuration (I) via the points II and III to the top of the energy barrier is reflected itself in the corresponding density distributions: each density crest observed at $\Theta=0°$ changes with increasing angle Θ more and more into a density peak. The maxima are thereby shifted towards the individual nuclei, i.e., we observe a density maximum close to the position of each nucleus and between both nuclei. In addition, each density peak develops a shoulder that decreases rapidly with further increasing angle Θ. The redistribution of the density from the parallel configuration to the top of the potential barrier of the 2_u PES is illustrated in Figs. 7(a) II and III for $\Theta=15°$ and 30°, respectively. Since both density peaks are always separated by a valley, the probability of finding the electron close to the internuclear axis and between both nuclei decreases rapidly with increasing angle Θ and reaches its minimum at $\Theta\approx35°$, which corresponds to the top of the energy barrier. After passing the ridge, the shape of the distribution changes dramatically. In addition to the inner maxima we now observe the formation of two outer density peaks that are separated by nodes from the other maxima. These outer maxima increase rapidly within a certain range of values of Θ, while the inner maxima decrease. At $\Theta=45°$, the outer maxima are the global density maxima and the height of the inner density peaks is roughly half that of the outer maxima [see Fig. 7(a) IV]. With further increasing angle Θ the two outer maxima start to decrease, while the inner maxima now begin to increase [cf. Fig. 7(a) V]. At the orthogonal configuration all density peaks, the inner as well as the outer maxima are located on the internuclear axis, which points along the x axis. In addition, the inner maxima are again the global maxima. The existence of two large density maxima between both nuclei is the reason for the observed potential well around the orthogonal equilibrium configuration. However, since these two inner maxima are separated by a node line along the z axis, the screening of the nuclear charges is incomplete, i.e., the corresponding potential well is, in comparison to that of the bonding 2_g state, much flatter. Finally, we remark that the node line of the 2_u density distribution along the z axis ($x=0$) at $\Theta=90°$ reflects the ungerade parity of the state considered. As we shall see below, this feature occurs also for the density distribution of

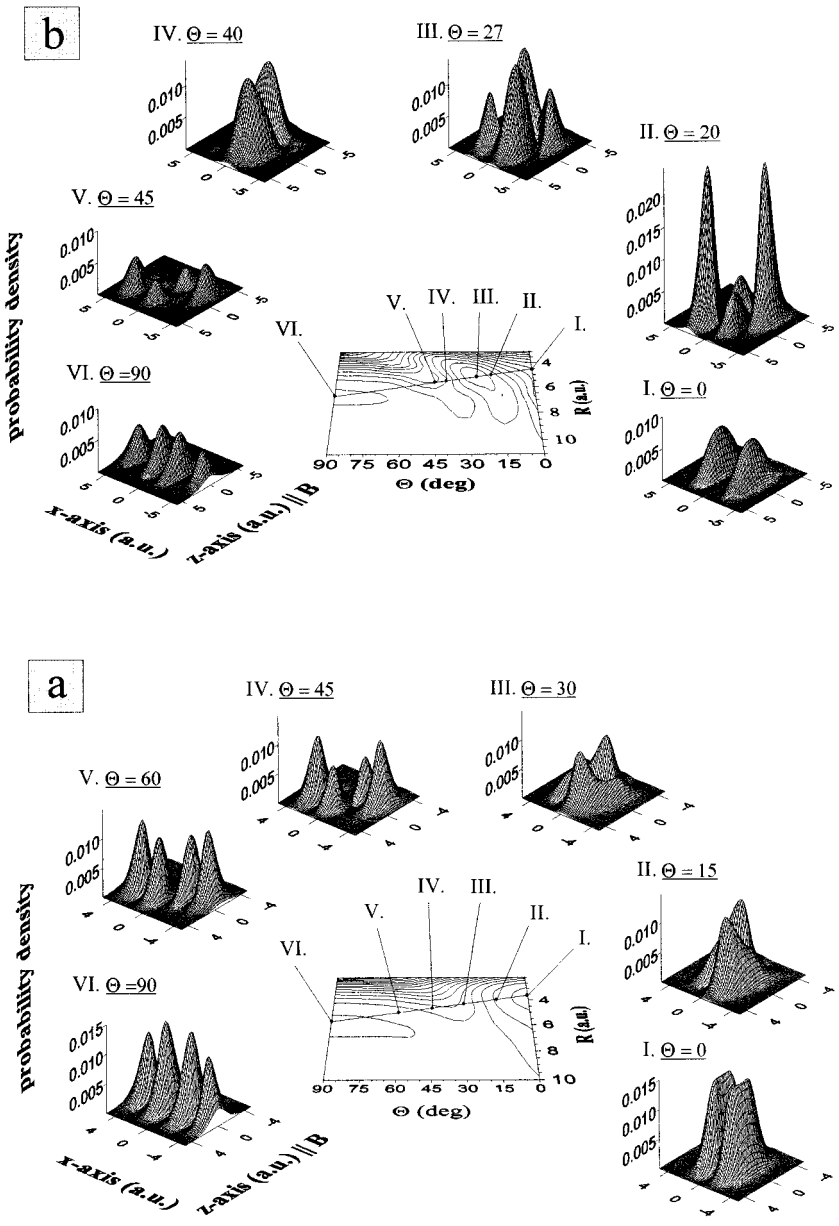

FIG. 7. Contour plots and the electronic probability distributions for selected values (R,Θ) in nuclear configuration space. (a) Contour plot of the PES of the 2_u state and the electronic densities at $\Theta=0°$, 15°, 30°, 45°, 60°, and 90°. (b) Contour plot of the PES of the 3_u state and the electronic densities at $\Theta=0°$, 20°, 27°, 40°, 45°, and 90°. (See the indicated points on the straight lines on the individual contour plot.)

the 3_u state at the orthogonal configuration.

The redistribution of the electronic density for the 3_u state with varying angle Θ is illustrated in Figs. 7(b) I–VI. The path we have chosen in order to investigate the changes of the probability density is recorded on the contour plot of the corresponding 3_u PES shown in the center of Fig. 7(b). Again we start our investigation at the parallel configuration $\Theta=0°$ and $R=4.57$ [see Fig. 7(b) I]. As already mentioned in Sec. IV C 1, the energy curve that belongs to the 3_u PES at $\Theta=0°$ consists, due to the higher symmetry, of two parts: the upper part from $R=0$ to $R\approx6.7$ belongs to the bonding $1\phi_u$ state, which possesses its equilibrium internuclear distance at $R=5.79$ [29], whereas the lower part ranging from $R\approx6.7$ to $R\rightarrow\infty$ belongs to the so-called antibonding $1\delta_u$ state. The density distribution shown in Fig. 7(b) I therefore belongs to the bonding state $1\phi_u$. The shape of this density distribution is very similar to that of the $1\delta_g$ and $1\pi_u$ states considered above. However, the conical intersection of the 3_u PES with the upper 4_u PES leads to a strong repulsion of the 3_u and 4_u PES if we change the parallel configuration to small, nonvanishing angle Θ [cf. Fig. 6(b)]. This conical intersection and surface repulsion, which are effects due to vibronic coupling, lead to the purely repulsive behavior of the 3_u PES around $\Theta=0°$ (see also the discussion of the 2_g PES). If we further incline the internuclear axis with respect to the magnetic field and choose $\Theta=20°$, the 3_u PES is again energetically well separated from both the lower 2_u and the upper 4_u PES and the corresponding density distribution is again an indicator of the topological properties of the 3_u PES. This situation is illustrated in Fig. 7(b) II. The density distribution possesses two strongly peaked maxima, each located close to an individual nucleus. In addition, we observe two local maxima, separated by nodes and located close to the internuclear axis and between both nuclei. The height of the local maxima is roughly five times smaller than the maximum values of the global density peaks. This electronic probability density exhibits a relatively low probability of finding the electron close to the internuclear axis between both nuclei and reflects, therefore, the behavior of the corresponding 3_u PES at $\Theta=20°$; i.e., this configuration is located still rather

far from the bottom of the two-dimensional potential well, which contains the global minimum of the 3_u PES.

With increasing angle Θ the global density peaks decrease rapidly while the absolute values of the local maxima increase. At the global equilibrium position of the 3_u PES, i.e., at $R=5.2$ and $\Theta=27°$, the density peaks that formerly were the global maxima are now local maxima and are located close to the nuclei [see Fig. 7(b) III]. The local maxima at $\Theta=20°$ [cf. Fig. 7(b) II] have now become the global density maxima, but they are still located close to the internuclear axis between both nuclei. In addition, always one pair of global and local maxima is connected via a saddle point; the position of the corresponding saddle point of each double peak is very close to an individual nucleus. Both double peak density structures are separated by a valley, i.e., by a node. Therefore, in comparison with the situation at $\Theta=20°$ [Fig. 7(b) (II)], we observe at $\Theta=27°$ an enhanced electronic density close to the internuclear axis and between both nuclei. This is the reason for the formation of a two-dimensional potential well in the 3_u PES around the configuration $R=5.2$, $\Theta=27°$.

Let us continue our journey along the indicated line on the contour plot of Fig. 7(b) and climb up the potential barrier that separates the two wells of the 3_u PES. We observe that the local maxima of the corresponding density distribution have disappeared. At $\Theta=40°$ [Fig. 7(b) IV], the global density peaks have kept their positions close to the internuclear axis between both nuclei, but have become broader. This density distribution suggests that the corresponding 3_u PES exhibits attractive behavior in the vicinity of the point $R=5.5$, $\Theta=40°$ (note that we are still inside the potential well, which contains the global energy minimum of the 3_u PES). However, since the ridge of the potential barrier represents the curve in nuclear configuration space where the upper 4_u PES comes closest to the 3_u PES, we expect the density distribution to change dramatically if we further incline the internuclear axis with respect to the magnetic field by a few degrees. In Fig. 7(b) V the electronic density distribution at $R=5.62$ and $\Theta=45°$, which corresponds to a position on the ridge of the potential barrier, is illustrated. We observe four flat maxima separated from each other by nodes. The global outer maxima are centered in the vicinity of the individual nuclei while the two inner local density peaks are located close to the internuclear axis between both nuclei. With increasing angle Θ, each peak moves towards the x axis. Simultaneously the outer density maxima decrease while the inner density peaks increase. At $\Theta=90°$, i.e., for the orthogonal configuration, all density peaks lie on the internuclear axis [see Fig. 7(b) VI]. The outer maxima are now the local ones and are separated by nodes from the inner maxima. The inner density peaks are similar to the corresponding density distribution of the 2_u state at $\Theta=90°$, the global maxima of the electronic density distribution, and are located exactly between both nuclei. The positions of the nuclei are $|x|=3.33$ and $z=0$. Analogous to the discussion of the density distribution of the 2_u state for the orthogonal configuration, we conclude for the 3_u state at $\Theta=90°$ that the strongly enhanced electronic density between both nuclei leads to an efficient screening of the nuclear charges and consequently to the formation of the observed two-dimensional potential well around the orthogonal equilibrium configuration. However, because of the occurrence of a node line along the z axis, the corresponding potential well is not very well pronounced.

V. CONCLUSION

In the present paper we have studied the ground as well as several excited magnetically dressed states of the H_2^+ ion for arbitrary orientations of the internuclear axis with respect to the magnetic-field axis. The key ingredient for our extensive numerical calculations of the molecular electronic states and potential-energy surfaces in the fixed nuclei approximation was a recently established and optimized basis set of generalized atomic orbitals.

In the first part of our investigation we studied the six lowest gerade and ungerade states of the H_2^+ ion in a strong magnetic field $B=1.0$ with gerade z parity at $\Theta=90°$. The potential-energy curves of the gerade states, i.e., the $1_g^+,\ldots,6_g^+$ states, possess well-pronounced potential wells. The depths of these wells decrease with increasing degree of excitation. The potential-energy curves of the ungerade states, i.e., the $1_u^+,\ldots,6_u^+$-states, exhibit also potential wells. However, in contrast to those of the gerade states, the wells of the magnetically dressed ungerade states are much flatter and their depths increase with increasing degree of excitation. By a harmonic approximation of the wells encountered we could show that, with the exception of the well of the 1_u^+ state, the vibrational ground-state energy is much smaller than corresponding depths of the wells and therefore many vibrational states exist in these wells.

Since the angle Θ between the internuclear and magnetic-field axes is an additional degree of freedom that, depending on the field strength, has rotational and/or vibrational character, we have to take into account this degree of freedom in order to investigate the global binding properties of the states considered. In the central section (Sec. IV) of the present paper we therefore investigated the local as well as global topological properties of the PES of several gerade and ungerade electronic states. First of all, we considered the PES of the gerade and ungerade ground states of the H_2^+ ion in a magnetic field $B=1.0$. Since the global properties of both states were already investigated in previous papers, we compared our data with the literature and obtained excellent agreement.

Next we studied the PES of the first two excited magnetically dressed gerade states of the H_2^+ ion, i.e., the 2_g and 3_g states, in the same strong field $B=1.0$. The 2_g PES and the 3_g PES exhibit their global minimum at $\Theta=90°$. By a harmonic approximation of the corresponding two-dimensional potential wells around the orthogonal equilibrium configuration we could show the existence of a large number of vibrational states in these wells. The 2_g and 3_g states are therefore examples of stable molecular states with a stable equilibrium configuration at $\Theta=90°$. The reason for this behavior was, in both cases, shown to be the strong redistribution of the probability density if we turn from the parallel to the orthogonal configuration; we observe the formation of a global probability density peak between the two nuclei, which reaches its maximum at $\Theta=90°$. Due to a node line along the internuclear axis in the corresponding density distribution of both states at $\Theta=0°$, such a global density maximum between the

two nuclei is not possible for the parallel configuration. In addition, at $\Theta=0°$ the lower 2_g PES conically intersects the upper 3_g PES. In the vicinity of this intersection vibronic coupling effects are important and the 2_g and 3_g states are strongly coupled via the nuclear motion. Hence the additional two-dimensional potential well of the 3_g PES around the parallel configuration does not provide a stable configuration.

Finally, we investigated the local as well as global topological properties of the 2_u and 3_u PESs. The 2_u PES possesses two minima: the global minimum occurs at $\Theta=0°$ and a further local minimum is located at $\Theta=90°$. The corresponding two-dimensional potential wells are separated by a potential barrier. In each potential well there exists a large number of vibrational states. Therefore, the 2_u state is an example of a double-well state: it possesses two stable molecular configurations at $\Theta=0°$ and 90°. The reason for the formation of the potential wells around the parallel and orthogonal equilibrium configuration is again the fact that the electronic probability density distribution at these distinct positions exhibits maximal values of the global density peaks located between the two nuclei and close to or on the internuclear axis.

The equilibrium configurations of all stable molecular states considered so far are located at positions of higher symmetry. This picture changes if we consider the 3_u state, which exhibits its global minimum at $\Theta=27°$. There exist a large number of vibrational states in the corresponding well and therefore the 3_u state is an example of a stable molecular state with a strongly lowered symmetry at its equilibrium configuration. Apart from the global minimum, the 3_u PES possesses also a second flat potential well around a local minimum at $\Theta=90°$. This flat potential well also contains a large number of vibrational states, i.e., the orthogonal equilibrium configuration is also a stable configuration of the excited 3_u state for $B=1.0$. Both minima of the 3_u PES again have their origin in the appearance of global density maxima close to the internuclear axis and between both nuclei.

With increasing degree of excitation, it is to be expected that the topological complexity of the adiabatic surfaces increases rapidly due to an increasing number of avoided crossings for $\Theta\neq0°,90°$. The present investigation yields the relevant data for a study of the nuclear dynamics (vibrational energies and oscillator strengths) in the potential-energy surfaces of the low-lying excited electronic states. The resulting theoretically calculated spectroscopic data might be helpful to analyze the observational data from the corresponding cosmic objects.

ACKNOWLEDGMENT

The Deutsche Forschungsgemeinschaft is gratefully acknowledged for financial support.

[1] J. P. Ostriker and F. D. A. Hartwick, Astrophys. J. **153**, 797 (1968); J. C. Kemp, J. B. Swedlund, J. D. Landstreet, and J. R. P. Angel, *ibid*. **161**, L77 (1970); J. Trümper, W. Pietsch, C. Reppin, B. Sacco, E. Kendziorra, and R. Staubert, Ann. N. Y. Acad. Sci. **302**, 538 (1977).

[2] C. P. de Melo, R. Ferreira, H. S. Brandi, and L. C. M. Miranda, Phys. Rev. Lett. **37**, 676 (1976).

[3] C. S. Lai and B. Suen, Can. J. Phys. **55**, 609 (1977); C. S. Lai, *ibid.* **55**, 1013 (1977).

[4] L. C. Melo, T. K. Das, R. C. Ferreira, L. C. M. Miranda, and H. S. Brandi, Phys. Rev. A **18**, 13 (1978).

[5] R. K. Bhaduri, Y. Nogami, and C. W. Warke, Astrophys. J. **217**, 324 (1977).

[6] J. M. Peek and J. Katriel, Phys. Rev. A **21**, 413 (1980).

[7] M. S. Kaschiev, S. I. Vinitsky, and F. R. Vukajlovic, Phys. Rev. A **22**, 557 (1980).

[8] J. Ozaki and Y. Tomishima, J. Phys. Soc. Jpn. **49**, 1497 (1980); Phys. Lett. **82A**, 449 (1981); J. Ozaki and Y. Hayashi, J. Phys. Soc. Jpn. **58**, 3564 (1989); J. Ozaki, *ibid*. **62**, 15 (1993).

[9] M. A. Maluendes, F. M. Fernandez, and E. A. Castro, Phys. Rev. A **28**, 2059 (1983).

[10] G. Wunner, H. Herold, and H. Ruder, Phys. Lett. **88A**, 344 (1982).

[11] J. C. le Gouillon and J. Zinn-Justin, Ann. Phys. (N.Y.) **154**, 440 (1984).

[12] M. Vincke and D. Baye, J. Phys. B **18**, 167 (1985).

[13] D. M. Larsen, Phys. Rev. A **25**, 1295 (1982).

[14] V. K. Khersonkij, Astrophys. Space Sci. **98**, 255 (1984).

[15] D. R. Brigham and J. M. Wadehra, Astrophys. J. **317**, 865 (1987).

[16] U. Wille, Phys. Rev. A **38**, 3210 (1988).

[17] Y. E. Lozovik and A. V. Klynchnik, Phys. Lett. **66A**, 282 (1978).

[18] M. Zaucer and A. Azman, Phys. Rev. A **18**, 1320 (1978).

[19] C. S. Warke and A. K. Dutta, Phys. Rev. A **16**, 1747 (1977).

[20] A. V. Turbiner, Pis'ma Zh. Eksp. Teor. Fiz. **38**, 510 (1983) [JETP Lett. **38**, 619 (1983)].

[21] S. Basile, F. Trombetta, and G. Ferrante, Nuovo Cimento **9**, 457 (1987).

[22] T. S. Monteiro and K. T. Taylor, J. Phys. B **22**, L191 (1989); J. Phys. **23**, 427 (1990).

[23] M. Demeur, P. H. Hennen, and M. Godefoid, Phys. Rev. A **49**, 176 (1994).

[24] A. M. Abrahams and S. L. Shapiro, Astrophys. J. **382**, 233 (1991).

[25] A. V. Korolev and M. A. Liberman, Phys. Rev. A **45**, 1762 (1992).

[26] D. Lai, E. E. Salpeter, and S. L. Shapiro, Phys. Rev. A **45**, 4832 (1992).

[27] P. Schmelcher and L. S. Cederbaum, Phys. Rev. A **37**, 672 (1988).

[28] U. Kappes and P. Schmelcher, J. Chem. Phys. **100**, 2878 (1994).

[29] U. Kappes, P. Schmelcher, and T. Pacher, Phys. Rev. A **50**, 3775 (1994).

[30] U. Kappes and P. Schmelcher, Phys. Rev. A **51**, 4542 (1995).

[31] J. E. Avron, I. W. Herbst, and B. Simon, Ann. Phys. (N.Y.) **114**, 431 (1978).

[32] B. R. Johnson, J. O. Hirschfelder, and K. H. Yang, Rev. Mod. Phys. **55**, 109 (1983).
[33] D. Baye and M. Vincke, Phys. Rev. A **42**, 31 (1990).
[34] P. Schmelcher, L. S. Cederbaum, and U. Kappes, in *Conceptual Trends in Quantum Chemistry* (Kluwer Academic, Dordrecht, 1994), pp. 1–51.
[35] P. Schmelcher, L. S. Cederbaum, and H. D. Meyer, Phys. Rev. A **38**, 6066 (1988); J. Phys. B **21**, L445 (1988).
[36] T. Detmer, P. Schmelcher, and L. S. Cederbaum, J. Phys. B **28**, 2903 (1995).
[37] P. Schmelcher and L. S. Cederbaum, Phys. Rev. A **41**, 4936 (1990).
[38] J. von Neumann and E. Wigner, Phys. Z. **30**, 467 (1929).
[39] J. E. Avron, I. W. Herbst, and B. Simon, Phys. Rev. A **20**, 2287 (1979).
[40] U. Kappes and P. Schmelcher, Phys. Lett. A **210**, 409 (1996).